ELSEVIER

Ceramics International 25 (1999) 331–338

CERAMICS INTERNATIONAL

Cavitation erosion of aluminas

W.J. Tomlinson [a], N. Kalitsounakis [b], G. Vekinis [b,*]

[a] *School of Natural and Environmental Sciences, Coventry University, Coventry CV1 5FB, UK*
[b] *Institute of Materials Science, NCSR "Demokritos", 15310, Greece*

Received 27 February 1998; accepted 1 July 1998

Abstract

Various aluminas were eroded in distilled water at 18°C using an ultrasonic facility operating at 20 kHz and with a peak-to-peak amplitude of 50 μm. The progress of erosion was measured by weight loss and the eroded surface was examined using a scanning electron microscope. Eight aluminas contained from 99 to 99.99% Al_2O_3 (considered pure) and three aluminas were debased by 4, 5 and 6% glass. The pure aluminas displayed incubation periods of about 15 to 30 min, linear erosion rates typically in the range 0.66 to 1.32 mg/h, failed in an intergranular manner, and gave linear erosion rates that were nearly independent of the grain size. The debased aluminas had incubation periods less than 15 min, linear erosion rates in the range 1.08 to 13.1 mg/h, failed mainly by intergranular fracture in the glass, and had linear erosion rates that were approximately proportional to the square of the average grain size. Steady state erosion occurred after the whole of the surface had been eroded to a depth approximately equal to that of the average grain size. The effects of porosity, purity of the alumina, and other microscopical details, are also discussed and a simple model is introduced which attempts to describe the results in terms of the fracture behaviour of the materials.

Keywords: B. Microstructure; C. Fracture; D. Alumina; Cavitation; Erosion

1. Introduction

Some of the most demanding applications of materials occur in hydraulic machinery. For example, valves, seals, bearing surfaces and impellers may operate in corrosive waters under cavitating conditions. Cavitation in the liquid occurs when the pressure is reduced below some critical value which results in the formation of a vast number of bubbles. These implode in another region of the liquid where the pressure is higher and the co-ordinated collapse generates a stress pulse ranging from a few hundred to over 1000 MPa [1]. The rapid repetition of the stress on the surface of materials in the immediate vicinity results in severe erosion [1]. Damage due to cavitation may be reduced by either altering the hydrodynamic profile to reduce the risk of cavitation, or by using a material that is more resistant to erosion [1]. If the cavitating liquid is corrosive, it is possible that the conjoint action of wear and corrosion may considerably increase the amount of damage. In the case of cast iron, corrosion due to a small amount of sodium chloride in the water accounted for only 1% of the damage whereas the erosion induced by cavitation accounted for nearly 80% of the damage [2].

Ceramics have a high resistance to wear and to corrosion. Generally, the main disadvantage to the wider use of ceramics is their low toughness, although, as pointed out by Brookes [3] when assessing the tribological applications of ceramic materials in water hydraulics, much of this limitation may be overcome in a large measure by inventive design rather than unimaginative substitution of materials.

Information on the cavitation erosion of ceramics is limited. In service it has been observed that cavitation erosion occurred on reaction-bonded silicon carbide used in a boiler feed pump [4], but such examples from industrial practice seem to be rare in the open literature. There have been two studies on the cavitation erosion of a range of engineering ceramics. Pennefather et al. [5] showed that a partially stabilised zirconia (PSZ) was more erosion resistant than a sialon, which was in turn more erosion resistant than an alumina. They also observed that the erosion resistance was extremely sensitive to the surface finish and the presence of microstructural defects. The cavitation erosion of various

* Corresponding author.

0272-8842/99/$20.00
PII: S0272-8842(98)00043-1

aluminas, zirconias, silicon carbide, silicon carbide–boron carbide composites, boron carbide and a sialon have more recently been investigated in detail, with particular attention directed towards measuring the incubation period [6].

Aluminas are commercially important and are among the most widely used structural cermaics. However, it is clear from the literature that the general properties and the wear resistance of aluminas greatly depends on the microstructure and the present work investigates the cavitation erosion behaviour of a range of aluminas with significantly different microstructures.

2. Experimental

Chemical compositions, microstructures and mechanical and physical properties of the ceramics tested are given in Tables 1 and 2, respectively. Specimen preparation and surface finish is known to have a marked influence on the erosion behaviour of ceramics [6] and thus particular care was taken to obtain a representative and reproducible surface. This was achieved by progressive diamond grinding, fine grinding and extended polishing down to 1 μm diamond on an automatic grinding/polishing machine. The grain size was determined on polished surfaces using the linear-intercept method.

Table 1
Composition, processing conditions and microstructure of the materials

Material[a]	Composition (wt%)	Sintering temperature (T_s) (°C)	Sintering time (t_s) (min)	Distribution of grains (%) in various size ranges (μm)							Average grain size (μm)	Interfacial material[e]
				2–3	4–6	7–10	11–15	16–20	21–30	31–40		
9999a	AKP30 (SUMITOMO)	1580	90	8	56	28	8	–	–	–	6	ND
9999b	AKP30	1580	360	–	26	36	20	14	4	–	11	ND
9975	99.75% AKP30, 0.25% MnO_2	1400	60	90	7	3	–	–	–	–	2	ND
997[b]	99.7% AKP30	1550	120	10	45	45	–	–	–	–	6	ND
995	99 + % Al_2O_3	Not disclosed	Not disclosed	–	12	18	20	20	23	7	17	ND
99a	99% AKP30, 1% MnO_2	1400	30	40	25	25	5	5	–	–	6	IP
99b	99% AKP30, 1% MnO_2	1400	60	25	35	30	5	5	–	–	6	IP
99c	99% AKP30, 1% MnO_2	1400	120	10	40	35	10	5	–	–	7	IP(S)
96	96% Al_2O_3	Not disclosed	Not disclosed	–	–	30	38	15	10	7	15	Glass
95[c]	95% Al_2O_3	1550	120	22	70	8	–	–	–	–	5	Glass
94[d]	94% Al_2O_3	1550	120	13	50	20	10	7	–	–	7	Glass

[a] Specimens fabricated in-house, except industrial ceramics 995 (Morgan Matroc) and 96 (Coors AD-96).
[b] Glass composition: MgO 0.12, SiO_2 0.07, Na_2O 0.04, CaO 0.02, $Fe_2O_3 < 0.1$, others < 0.01.
[c] Glass composition: SiO_2 3.0, MgO 1.5, CaO 0.16, Cr_2O_3 0.12, Na_2O 0.08, Fe_2O_3 0.03, others < 0.01.
[d] Glass composition: SiO_2 3.2, CaO 2.7, Na_2O 0.10, MgO 0.04, K_2O 0.04, Fe_2O_3 0.04, TiO_2 0.01.
[e] ND = no phases detected microscopically; IP = isolated unidentified phases; IP(S) = IP with one of the phases spinel; Glass indicates a substantial amount of glass present.

Table 2
Mechanical and physical properties of the materials

Material	Young's modulus (E) (GPa)	Macro-Hardness (HV5) (GPa)	Fracture toughness (K_{Ic}) ($MPam^{1/2}$)	Bulk density		Open porosity (%)	Closed porosity (%)	Total porosity (%)
				(g/cm^3)	(%)			
9999a	386	15.4	3.3	3.93	99.0	0.01	0.97	0.98
9999b	386	15.6	2.8	3.93	99.0	0.01	0.98	0.99
9975	380	15.4	3.4	3.80	95.6	2.31	2.06	4.37
997	380	16.7	3.4	3.90	98.4	0.00	1.64	1.64
995	330	13.3	NM	3.90	98.3	0.02	1.71	1.73
99a	370	14.8	3.7	3.85	96.9	0.15	2.90	3.05
99b	370	14.8	3.9	3.86	97.2	0.14	2.63	2.77
99c	370	15.2	2.9	3.91	98.5	0.00	1.50	1.50
96	303	10.7	NM	3.70	93.9	0.00	6.10	6.10
95	303	11.6	3.0	3.70	94.6	0.00	5.35	5.35
94	300	10.8	3.3	3.72	95.6	0.00	4.28	4.28

NM: not measurable due to premature microfracture.

An ultrasonic facility operating at 20 kHz and 50 μm peak-to-peak amplitude was used to erode the materials. The specimens were held in a rigid stainless steel jig attached to the ultrasonic titanium alloy anvil as used by Heathcock et al. [7] and others. Samples, of minimum thickness 5 mm and diameter approximately 20 mm, were immersed in 3–6 mm of a fresh charge of 800 ml of distilled water maintained at $18 \pm 1°C$ and the polished surface was positioned 1 ± 0.1 mm from the horn tip. This arrangement maintained a constant area of erosion (1.54 cm^2). The anvil tip was polished after every test to preserve reproducibility. Erosion kinetics were measured by mass loss using an analytical balance accurate to 0.1 mg. The incubation period was measured by periodically measuring the erosion every 1 min up to 15 min and every 5 min thereafter, until a weight loss of 0.1 mg was detected. This measured incubation period, which is only rarely determined, should be distinguished from the so-called nominal incubation period which is obtained by extrapolation of the linear erosion rate onto the time axis. Thereafter, the specimens were weighed every hour up to 15 h. Full details of the apparatus, calibration, materials and operating procedures are given in detail elsewhere [8].

3. Results and discussion

Erosion followed a uniform pattern of behaviour in all the materials tested. Typical curves of mass loss as a function of time for a pure alumina (997) and a debased alumina (94) are shown in Fig. 1 and details of all the erosion kinetics are given in Table 3. Firstly, there was an incubation period, defined here as the time when the weight loss was less than 0.1 mg. This point is not evident on the scale of the graphs and is tedious to determine precisely, but for the debased aluminas (94, 95 and 96), the incubation period was less than 15 min whereas for the other materials it was between 15 and 30 min. There then followed a period of irregular but overall accelerating rate of mass loss. Finally, there was a linear erosion rate region (LER) which extended over a considerable time and degree of damage. The linearity of the final rate enabled an estimate to be made of the rate using a limited number of tests on a second sample. It is seen that there is considerable scatter in the LER (Table 3). For convenience, a nominal incubation period (NIP) measured as the time when the linear region is extrapolated onto the time axis, is also obtained from the erosion data and included in Table 3.

The eroded surface of all the materials was examined in a scanning electron microscope in detail at each stage of the erosion process when the test was interrupted to determine the weight loss. A uniform pattern of damage occurred for each material and some representative details are shown in Fig. 2 for the progressive erosion of material 997 together with a schematic diagram of the erosion progress. It would seem from observations of the apparently uniform depth of the eroded surfaces, that erosion occurs in a layer-by-layer fashion. The initial surface containing a flaw is shown in the micrograph at position A in Fig. 2. After 30 and 45 min, the

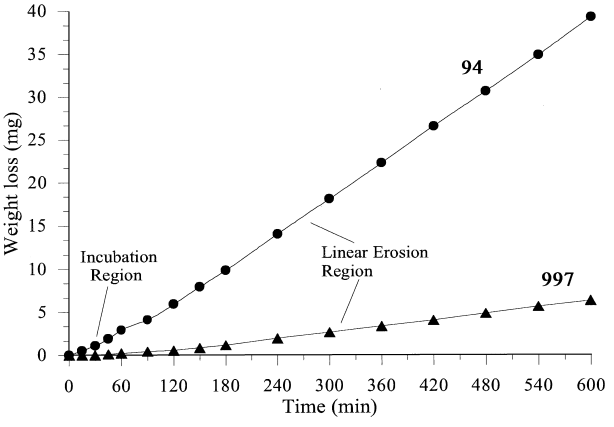

Fig. 1. Typical curves of mass loss vs time for a pure alumina (997) and a debased alumina (94).

Table 3
Results of the cavitation erosion experiments

Material	Nominal incubation period (NIP) (min)	Linear erosion rate (LER) (average)			Weight loss after 10 h (mg)
		(mg/h)	(mm^3/h)	Scatter (%)	
9999a	84	1.32	0.335	9.5	11.3
9999b	47	1.11	0.282	11.8	10.2
9975	36	1.20	0.257	22.2	11.1
997	97	0.69	0.177	9.1	5.8
995	35	6.72	1.723	38.3	62.3
99a	20	0.72	0.187	18.2	6.7
99b	29	0.84	0.218	33.3	7.9
99c	62	0.87	0.223	7.1	7.8
96	5	12.4	3.351	12.0	123
95	41	1.29	0.349	38.9	11.7
94	20	4.51	1.212	14.8	43.8

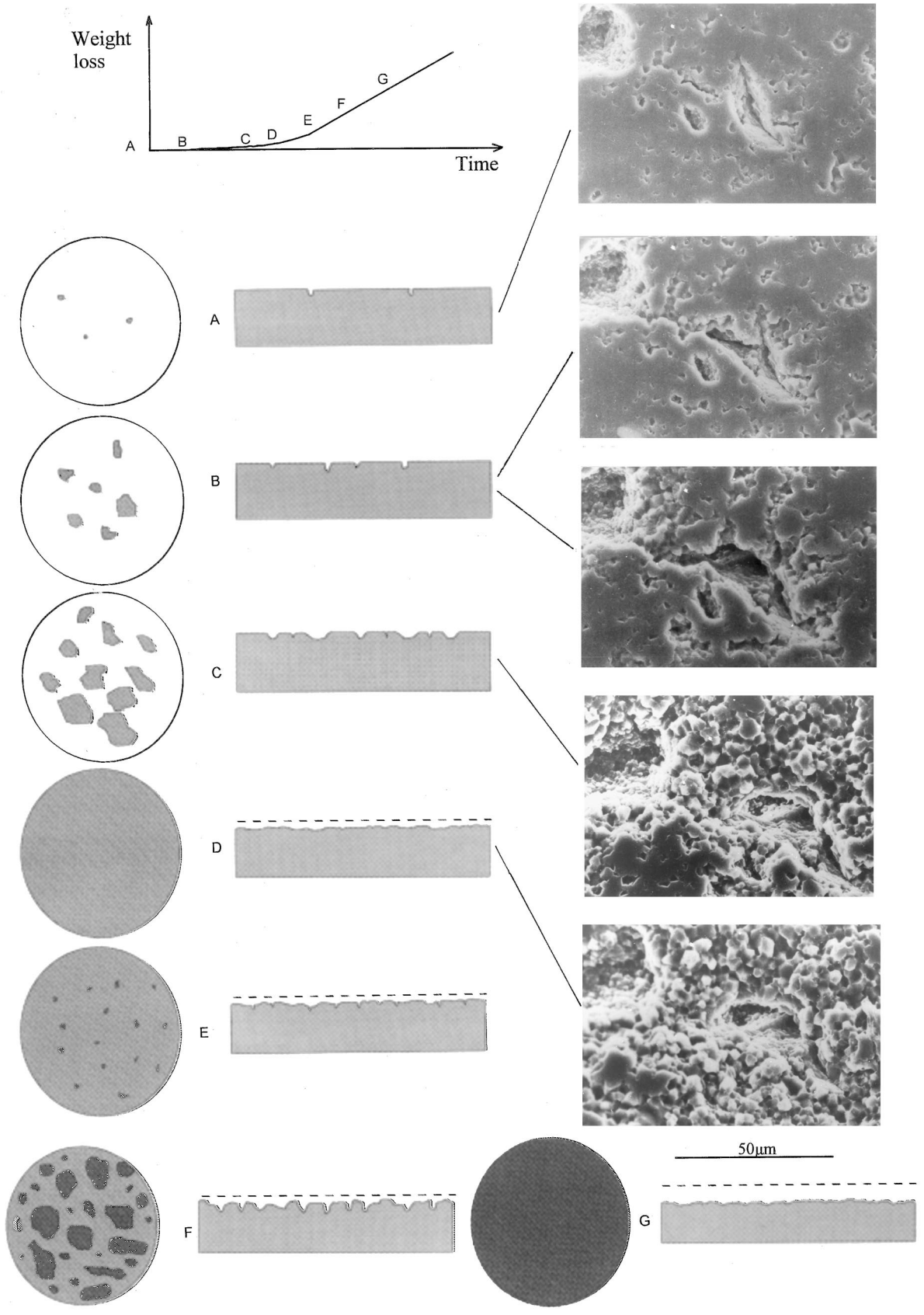

Fig. 2. Schematic represemtation of the typical progress of erosion with SEM micrographs of the surface of alumina 997 after various times and amounts of erosion. Erosion progresses in a layer-by-layer fashion.

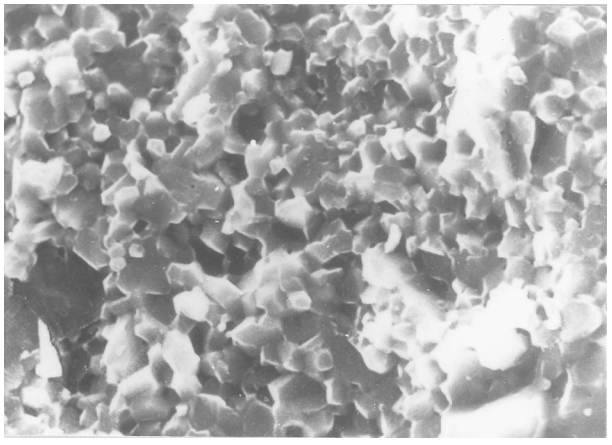

Fig. 3. SEM micrograph of alumina 9999a clearly showing the intergrannular nature of fracture (480 min; 7.5 mg).

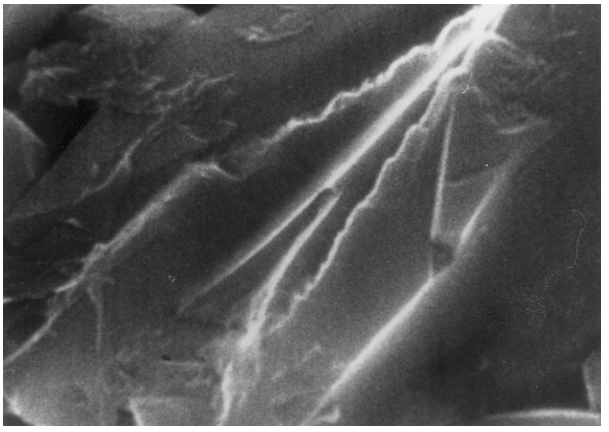

Fig. 4. SEM micrograph of transgranular fracture through the glassy phase in alumina 94 (240 min; 14.0 mg).

weight loss was less than 0.1 mg. Mass loss begun at the intersection of grain boundaries and pores (position and micrographs B) and this then extended to the general edges of the pores and over the surface (positions and micrographs C and D). This process repeated itself for the next layer of grains (positions E, F and G in Fig. 2). In particular there was no obvious cratering that is sometimes observed on metal surfaces eroded by cavitation and frequently ascribed to a liquid jet mechanism of erosion. Steady state erosion was almost entirely by intergrannular fracture (Fig. 3) but also, very rarely, by transgrannular fracture. A similar pattern was observed for all the pure aluminas. Material 995 was unusual inasmuch as it contained many abnormally large grains, but, despite their size, microfracture of the material was still largely intergrannular. These progressive SEM observations indicate that cavitating bubbles appear to attack preferentially the grain boundaries either by direct impingement and erosion or by shock wave reflection on the grain boundaries. This appears to indicate that the mechanism of material removal is different from that observed for metals.

The debased aluminas followed a similar pattern of damage. Typically fracture was intergrannular in the glass at the crystal/glass interface, but frequently, fracture occurred in the bulk of the intergranular glass (Fig. 4). There are however differences depending on the composition of the glassy phase. In flexure, high-CaO debased aluminas (94) fail predominantly intergranularly and high MgO-debased aluminas (95) fail predominantly transgranularly as noted before as well [9]. The mixed mode of fracture in both the high MgO and high CaO aluminas most probably reflect the different mode of deformation in cavitation erosion compared with that in flexure. The relatively large volume of glass in the debased aluminas allowed the fracture to be almost entirely in the glass, whereas the much smaller volume of intergranular material in the pure materials forces the crack to take a more tortuous and hence more energy absorbing path. However, erosion depends not only on the fracture path but also on the microchemistry. Thus the debased aluminas have similar amounts of glass and fracture modes but substantially different linear erosion rates (Table 3) indicating that, in these cases, the strength of the glass is an important factor.

The difficulties in modelling the cavitation erosion of ceramics have been discussed briefly above, and there is no established theory of the process. Material is removed from the surface of brittle ceramics predominantly by microfracture, which has led to a number of attempts at relating LER with the toughness of the material [6,11–13]. This is not the conventional quasi-static large-scale toughness. Ruff and Wiederhorn have emphasised the dynamic toughness ([11] p. 122), and others have emphasised the microstructural scale of toughness and the caution with which conventional toughness results should be applied to wear, erosion, and machining [12,13]. The present results do not show any obvious relation between the LER (Table 3) and the conventional toughness of the materials (Table 2) measured here by conventional fracture mechanics techniques.

Clearly the microstructure has a prominent influence on the erosion behaviour. In an ideal case the start of the steady state erosion might occur when a uniform layer of the material has been removed. Since fracture is predominantly intergranular, it may be that the erosion rate somehow depends on the grain size. Along these lines, a first-order approximation of LER may be obtained by consideration of the intergrannular layer-by-layer fracture mechanism that was observed. For the purpose of modelling the mass loss, the actual mechanism of energy input by cavitation (be it microbubble implosion, impingement, liquid microjet, etc.) is actually not important as long as it can be assumed that it is quasi-continuous and well distributed over the area under erosion.

As discussed above, the fracture mode is predominantly intergrannular in all cases: pure aluminas as well as debased aluminas, where fracture occurs through the interfacial glassy phase. There is only minimal evidence of partially worn or fractured grains. We can thus assume, with little error, that the material removed is in the form of whole grains fractured intergrannularly and that it is removed continuously. The Linear Erosion Rate (LER, as volume removed per unit time) is then, to a sufficient approximation, given simply by:

$$\mathrm{LER} = c_1 N d^3 + \Psi \tag{1}$$

where N is the average number of grains removed per unit time, d is the average grain size, c_1 a geometric constant of the order unity depending on the shape of the grains and Ψ a small contribution due to partly worn or fractured grains.

From the SEM observations, it appears that the limiting mechanism for cavitation erosion is microfracture as a result of stress concentrations that occur on the grain boundaries. If these contain appreciable amounts of interfacial glassy phase, which is much weaker than alumina, then the erosion rate is higher. The energy per unit time of the cavitating bubbles E is applied uniformly and continuously over the area under attack. In order for the above amount of material to be removed therefore, this energy needs to fracture on average the following intergrannular surface area per unit time:

$$c_2 N \pi d^2 \tag{2}$$

where c_2 is another geometric constant of the order 0.5, we have averaged the process over time, taken into account that 1/2 of the surface area of the grains need to be fractured to remove a grain completely and that fracture of one interface affects two grains. In fact this is probably an overestimation as some interfaces fracture under fast fracture conditions before they are worn. However, it is accurate enough for our purposes.

A constant fraction of the cavitation energy supplied is used for fracturing this area:

$$E = c_3 \gamma N d^2 \tag{3}$$

where γ is the fracture energy per unit area of fracture, which may be approximately identified with the intrinsic toughness of the interface. For ceramics with very little or no interfacial phase it is probably close to their toughness G_{Ic}. In the case of ceramics with appreciable interfacial glassy phase fracturing intergranularly, γ is identified with G_{Ic} of the glassy phase, suitably adjusted due to the constraining influence of the surrounding grains.

Solving for N and substituting in Eq. (1) we get:

$$\mathrm{LER} = C\frac{d}{\gamma} + \Psi \tag{4}$$

where C is a constant which depends on the grain shape and the energy applied to the system by the cavitating bubbles per unit time. If all testing conditions, such as frequency, amplitude, temperature, environment, etc., are held constant, then the energy input is also constant. Eq. (4) shows therefore that, under constant conditions, LER should depend only on d and γ.

The results appear, qualitatively, to confirm this simple model although more systematic work needs to be carried out to confirm it more accurately. Plotting LER vs d (Fig. 5) produces two distinct groups of materials; those with no glassy phase with a very small gradient and the debased materials containing substantial glassy phase with a larger gradient. From the gradients of the two curves, the fracture energies of the two groups can be calculated to be in the ratio of at least 1:15 which is in approximate agreement with the ratio of the calculated toughness of the pure aluminas studied in this work (their toughness G_{Ic} is calculated from the values of K_{Ic} and E to be about 0.02–0.04 kJ/m^2) and that for the toughness of glass of about 0.002–0.005 kJ/m^2.

The effect of porosity on the mechanical properties of brittle ceramics has been intensely researched and, for example, the strength of alumina has been shown to decrease as the porosity increases ([10] p. 223). The decrease in strength occurs more rapidly than the decrease in density because the pores concentrate the stresses unevenly across the true cross-section. This behaviour is frequently expressed as $S = S_o \exp(-bP)$ where S is the strength, P is the porosity, and S_o and b are constants ([14] p. 809). We may thus expect that porosity would be of prime importance in the early stages of erosion where the pores on the surface may concentrate the stresses due to cavitating bubbles and

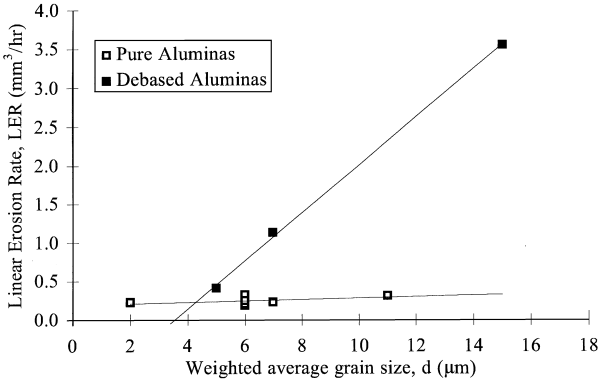

Fig. 5. Linear erosion rate (LER) as a function of weighted average grain size. The materials fall into two distinct groups with a ratio of gradients of at least 1:10.

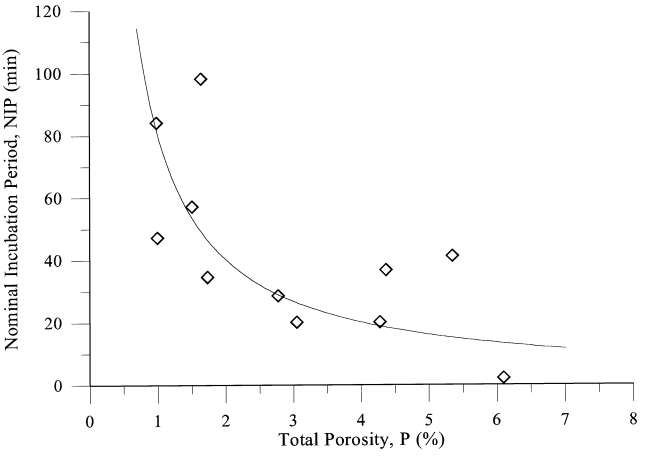

Fig. 6. Nominal incubation period, (NIP) as a function of porosity (P). The line is a hyperbolic fit to the results of the form $NIP = C/P$ with $C = 80$ min.

thus have a direct influence on the nominal incubation period NIP. A relation between NIP and porosity may thus be expected to have a similar empirical form. In fact, a better fit of the results is obtained (Fig. 6) by a simple hyperbolic relationship of the form $NIP = C/P$ where C is a constant of approximate value 80 min. This indicates that initiation of the linear erosion region may be delayed in aluminas with low porosity, and possibly in other ceramics, and NIP may thus be of value in describing the cavitation erosion kinetics in the initial stages.

There are a large number of composition and microstructural variables in the aluminas investigated, and these, combined with the scatter inherent in determining the cavitation erosion behaviour of ceramics and the absense of full details of the microchemistry and microstructures of all the materials, limit the extend of the conclusions we can draw. However, a number of points may be made. It is seen that the 99.5% Al_2O_3 specimen had an abnormally large grain size, and this appears to be responsible for its abnormally high erosion rate. The different sintering times of the 99a, 99b, and 99c materials had a small effect on either the grain size or the linear erosion rate, despite a substantial reduction in the porosity from 3.05 to 1.50%. From an applications point of view, the erosion resistance of the commercial 95% alumina is outstanding and this clearly indicates that although a large amount of intergranular glass may lower the erosion resistance of an alumina, by a careful control of the microstructure and microchemistry it is possible to maintain a high level of erosion resistance.

Cavitation erosion is sensitive to the testing conditions. A previous study [6] used the same test conditions as the present work, and hence results may be at least semi-quantitatively comparable. In that study [6] a 99.9% commercial alumina had an incubation period of 150 min and a linear erosion rate of 0.49 mg/h. These are better than those obtained in the present work. In particular the incubation period is much higher than the 15 to 30 min obtained with any of the aluminas. This reinforces again the point that the erosion behaviour of aluminas do not depend simply on the purity of the material but in a complex way on both the microchemistry and microstructure.

4. Conclusions

Various commercial aluminas and specially prepared aluminas were investigated for their cavitation erosion behaviour. Eight of the materials had a purity above 99% (considered pure) and three contained between 4 and 6% glass (debased). All the materials followed the usual pattern of erosion damage with time. The incubation periods of the pure aluminas and the debased aluminas were from 15 to 30 min and less than 15 min, respectively, and the nominal incubation period, NIP, appeared to be hyperbolically related to the total porosity of the material. The linear erosion rates (LER) of the pure aluminas and the debased aluminas were in the ranges 0.66 to 1.32 mg/h and 1.08 to 13.1 mg/h, respectively. A pure alumina with an abnormally large grain size had LER = 7.80 mg/h. The transition to the steady state period of erosion occured when the whole surface had been eroded to a depth approximately equal to the average grain size. In the pure aluminas material started to be lost at grain boundaries associated with pores, thereafter material was lost by intergranular fracture and the removal of whole grains. In the debased aluminas material started to be lost from the glass at a glass/alumina interface, thereafter material was lost mainly through fracture in the intergranular glass with occasional transgranular fracture in the alumina grains. A simple model for LER based on the fracture energy of the interface is supported by the observations and indicates that LER is proportional to the grain size and

inversely proportional to the fracture energy of the interface.

References

[1] A. Karimi, J.L. Martin. Inter. Metals Rev. 31 (1986) 1–26.
[2] W.J. Tomlinson, M.G. Talks. Tribology Int. 22 (1989) 195–203.
[3] R.J. Brook. Proc. Br. Ceram. Soc. 32 (1982) 7–24.
[4] S. Parrott. Metals Materials 6 (1990) 207–213.
[5] C. Pennefather, S.E. Hankey, R. Hutchings, A. Ball. Mater. Sci. Eng. A105/106 (1988) 389–394.
[6] W.J. Tomlinson, S.J. Matthews. Ceram. Int. 20 (1994) 201–208.
[7] C.J. Heathcock, B.E. Protheroe, A. Ball, A., Proc. 5th Int. Conf. on Erosion by Liquid and Solid Impact, Cambridge, UK, September, 1979, pp. 631–638.
[8] N. Kalitsounakis, Cavitation erosion of aluminas, M.Phil. thesis, Coventry University, Coventry, UK, 1995.
[9] C.A. Powell-Dogan, A.H. Heuer. J. Am. Ceram. Soc. 73 (1990) 3684–3689.
[10] R.L. Coble, Effect of microstructure on mechanical properties, in: W.D. Kingery (Ed.), Ceramic Fabrication Processes, Wiley, New York, 1958.
[11] A.W. Ruff, S.M. Wiederhorn, Erosion by solid particle impact, in: Treatise in Materials Science and Technology, Vol. 16, Erosion. Academic Press, New York, 1979.
[12] D.B. Marshall, B.R. Lawn, R.F. Cook. J. Am. Ceram. Soc. 70 (1987) C139–C140.
[13] S.-J. Cho, B.J. Hockey, B.R. Lawn, S.J. Bennison. J. Am. Ceram. Soc. 72 (1989) 1249–1257.
[14] W.D. Kingery, H.K. Bowen, D.R. Uhlmann, Introduction to Ceramics, 2nd Edition. Wiley, New York, 1976.